

# Analysis of trilinear Higgs self coupling in Two Higgs Doublet model at lepton collider

Ijaz Ahmed,<sup>1,\*</sup> M. Danish Aslam,<sup>1,†</sup> Taimoor Khurshid,<sup>2,‡</sup>

Jamil Muhammad,<sup>3,§</sup> and Shamona Fawad Qazi<sup>4,¶</sup>

<sup>1</sup>*Federal Urdu University of Arts, Science and Technology, Islamabad Pakistan*

<sup>2</sup>*International Islamic University Islamabad Pakistan*

<sup>3</sup>*Sang-Ho College, and Department of Physics,*

*Konkuk University, Seoul 05029, South Korea*

<sup>4</sup>*Quaid-i-Azam University, Physics Department Islamabad Pakistan*

## Abstract

Reconstruction of Higgs potential relies on trilinear Higgs self-coupling which further depends upon the Higgs boson masses. In this study, computational analysis of neutral Higgs bosons  $h$ ,  $H$  and  $A$  is carried out within the parameter space of Two Higgs Doublet Model (2HDM) type-I in exact alignment limit of  $\sin(\beta - \alpha) = 1$  at compact linear collider. Assuming Compact Linear Collider (CLIC) scenario where the electron-positron beams will be collided at  $\sqrt{s} = 1.5$  TeV. Two different values of predicted integrated luminosities are used in our calculations,  $1000 \text{ fb}^{-1}$  and  $2500 \text{ fb}^{-1}$ . Three signal processes  $e^+e^- \rightarrow Zh h \rightarrow jj b \bar{b} b \bar{b}$ ,  $e^+e^- \rightarrow Z H H \rightarrow jj b \bar{b} b \bar{b}$  and  $e^+e^- \rightarrow Z h h \rightarrow jj b \bar{b} b \bar{b}$  are selected for analysis. The polarized colliding beams are used to enhance the signal production cross-section. Low  $\tan \beta$  and equal Higgs masses regime is chosen in favor of Hadronic decay of  $Z$  boson and  $H \rightarrow b \bar{b}$ . Different signal scenarios are selected and event generation is performed for each process separately. The  $W$  and  $Z$  boson, as well as top quark backgrounds are analyzed. Signal significance is computed at each Higgs mass hypothesis for three signal processes. After a comprehensive study, we did not find sizeable amount of signal events on top of the background but still, signal significance is found to be larger than 1, without taking into account the detector effects and systematics. The maximum calculated value of signal significance is observed to lie in the range of  $150 \leq m_H \leq 250$  GeV for  $Z h h$  while for  $Z H H$  the range is  $175 \leq m_H \leq 200$  GeV at  $1000 \text{ fb}^{-1}$  and  $175 \leq m_H \leq 225$  GeV region at  $2500 \text{ fb}^{-1}$ . Similarly, for  $Z A A$  process, the significance is highest at  $m_A = 175$  GeV for both  $1000$  and  $2500 \text{ fb}^{-1}$ .

PACS numbers: 12.60.Fr, 14.80.Fd

Keywords: 2HDM, Collider, Coupling, significance.

\*Electronic address: [ijaz.ahmed@fuuast.edu.pk](mailto:ijaz.ahmed@fuuast.edu.pk)

†Electronic address: [danishaslam00786@gmail.com](mailto:danishaslam00786@gmail.com)

‡Electronic address: [taimoor.khurshid@iiu.edu.pk](mailto:taimoor.khurshid@iiu.edu.pk)

§Electronic address: [mjamil@konkuk.ac.kr](mailto:mjamil@konkuk.ac.kr)

---

<sup>¶</sup>Electronic address: shamona@qau.edu.pk

## I. INTRODUCTION

Giving mass to fermions by Electroweak Symmetry Breaking (EWSB) mechanism is the key feature of SM Higgs sector [1–3]. Quadratic scalar potential along with scalar Higgs field handles the EWSB mechanism. In the Higgs mechanism, the neutral constituent of an iso-doublet scalar field attains some vacuum expectation value (VEV) which results in masses of fermions and vector bosons while preserving the gauge symmetry of  $SU(2) \times SU(1) \times U(1)$  transformation. In SM, coupling of fermions and vector bosons with Higgs is a function of their corresponding masses that's why their mass is the only free parameter in the Higgs sector. Higgs-pair production is important, since it can be used for the detection of Higgs self-coupling. Discovering deviations from its SM prediction provides indirect possibilities for finding new physics and the existence of heavy new particles. Measurement precision in the range of 20% could allow observation of deviations from the SM and can reveal extended Higgs sectors [4]. The Higgs sector of SM is extended by incorporating another Higgs doublet of symmetry  $SU(2)$ . This modification steers to a 2HDM [5–12] that shows very interesting phenomenological attributes. Such as, in the parameter region of 2HDM, in which the theory of Electroweak Baryogenesis is possible, a minimal expected deviation from the SM is 20% [13]. Two presumed  $SU(2)$  Higgs doublets of 2HDM comprise of eight degrees of freedom. Vector bosons absorb three of them and the remaining five steer towards the supposition of five Higgs bosons. One is considered as the uncovered SM Higgs boson and all others are treated as free parameters that are not yet discovered. In 2HDM, there are five Higgs bosons: two charged ones ( $H^\pm$ ), two CP-even neutral Higgs  $h$ ,  $H$  and one CP-odd neutral  $A$ . Due to the addition of extra scalar doublet, 2HDM has richer phenomenology than SM.

In order to establish the EWSB mechanism, the scalar potential of the Higgs field needs to be constructed such as to obey orthogonality. However, that requires making measurements of the triple and quadratic self-couplings,  $g_{\phi\phi\phi}$  and  $g_{\phi\phi\phi ss\phi}$  respectively. The double Higgs-strahlung ( $e^-e^+ \rightarrow Z\phi\phi$ ) along with WW double-Higgs fusion makes it possible to measure the triple Higgs self-coupling with significant precision in the SM [14–17]. On the other hand, measuring Higgs self-coupling allows us to reconstruct the Higgs potential, which is the most conclusive test of the EWSB mechanism. If the scalar sector is extended like the 2HDM, determining the self-couplings, as well as the Higgs potential, could be a complicated task. In 2HDM, there are in a total of 8 trilinear Higgs self-couplings. A similar attempt was made earlier, to find out at what extent the trilinear Higgs couplings could be probed by studying various Higgs boson pairs associated with the Z boson in reference [18]. However, the processes and the region of interest differ from our

study and most importantly, the motivation for the free parameters of the model does not hold the basic theoretical constraints (perturbativity and unitarity) of the model which is claimed otherwise. Some of the couplings are studied through the double and triple Higgs boson production in reference [19, 20]. Besides, triple and quartic Higgs couplings have been studied at the linear colliders in the context of the MSSM in reference [21–25]. In this work, we analyze various scattering processes in  $e^-e^+$  collider to conclude whether all these Higgs self-couplings can be determined. In this aim, the correlation between these couplings and scattering processes is examined. Cross-sectional values of double Higgs production in SM are insignificant, but Higgs self-coupling measurement required by new physics is quite challenging and enhanced by sizeable factors. Because of multi-jet final states, the measurement places many challenges on detector technologies and event reconstruction techniques. Hence, it is challenging to investigate the possibilities of measuring the Higgs self-coupling at particle colliders. Many experiments were carried out at LHC that gave many beneficial results. But a more precise machine like a lepton collider is required for the thorough study of Higgs particle and its properties. Since, the initial state is well defined in a lepton collider, we can easily determine the four momenta from the products which helps in reconstructing the event. There are a variety of lepton colliders around the world: the Circular Electron-Positron Collider (CEPC) based in China, having beam energy of 120 GeV [26–28], the proposed Future Circular Collider (FCC-ee) [29] by CERN [30], the International Linear Collider (ILC) with beam energy of 500 GeV extendable to 1TeV, based in Japan [31] and Compact Linear Collider (CLIC) having beam energy of 380 GeV and proposed beam energies of 1.5 and 3 TeV based in CERN [32]. All of these lepton colliders will be Higgs factories and thus the best choice to study Higgs and its properties and can also interpret LHC results.

This study is related to  $h$ ,  $H$ , and  $A$  Higgs bosons with focus on the visibility of these particles in 2HDM parameter space in a SM-like regime. The 2HDM form contains flavor-changing neutral currents (FCNCs) which is in contradiction with the experimental results. These FCNCs can be avoided by imposing  $Z_2$ -symmetry. Four types of 2HDM arise whereas different couplings of fermions with Higgs result in flavor conservation. This  $Z_2$ -symmetry is broken by a dimension two operator  $\phi_1^\dagger\phi_2$  or  $\phi_2^\dagger\phi_1$  with the addition of a soft symmetry breaking term  $m_{12}^2$ . The exact alignment limit and equal mass scenario make signal processes independent of  $\tan\beta$ . Low  $\tan\beta$  value is chosen in favor of hadronic decay of  $Z$  boson and  $H \rightarrow b\bar{b}$ . For these scattering processes, contributing backgrounds are  $WW$ ,  $ZZ$ ,  $t\bar{t}$  and  $ZZZ$ . Different benchmark points are chosen in 2HDM parameter space and event generation is done for each scenario. We expect this proposed analysis, a tool to serve those who are working on the observability of neutral Higgs boson via

Triple Higgs coupling. In section 2, a brief description of two Higgs doublet model (2HDM) is given. In section 3, trilinear Higgs coupling in SM and 2HDM is discussed. In section 4, details of computational tools are given. In sections 5 and 6, Higgs decays and procedure for selection of signal scenarios are discussed, respectively. In section 7, signal and background processes are discussed. Results are shown in sections 8 to 11 and section 12 gives the conclusion.

## II. TWO HIGGS DOUBLET MODEL

In 2HDM, another  $SU(2)_L$  doublet with same hypercharge as the first one, i.e.  $Y = 1/2$  is added. Two  $SU(2)$  Higgs doublets in general form are given as [33],

$$\langle \phi_i \rangle = \begin{pmatrix} \phi_i^\dagger \\ \frac{1}{\sqrt{2}}(\nu_i + \rho_i + i\eta_i) \end{pmatrix} \quad (1)$$

where  $i = 1, 2$ . Let us assume that direction of vacuum expectation value is along CP-even neutral Higgs field [34], then  $\langle \rho_1 \rangle = \nu_1$  and  $\langle \rho_2 \rangle = \nu_2$ , which defines  $\tan \beta = \nu_2/\nu_1$  and  $\nu = \sqrt{\nu_1^2 + \nu_2^2} = (\sqrt{2}G_F^0)^{-1/2} = 2M_W/g = 246$  GeV. Both vacuum expectation values are real due to  $U(1)_\gamma$  invariance and taken as positive without losing generality [45]. The most general form of the gauge invariant and renormalized Higgs potential in terms of generic basis is [36],

$$\begin{aligned} V(\phi_1, \phi_2) = & m_{11}^2(\phi_1^\dagger \phi_1) + m_{22}^2(\phi_2^\dagger \phi_2) - \{m_{12}^2(\phi_1^\dagger \phi_2) + h.c\} + \frac{1}{2}\lambda_1(\phi_1^\dagger \phi_1)^2 + \frac{1}{2}\lambda_2(\phi_2^\dagger \phi_2)^2 + \\ & \lambda_3(\phi_1^\dagger \phi_1)^2(\phi_2^\dagger \phi_2)^2 + \lambda_4(\phi_1^\dagger \phi_2)^2(\phi_2^\dagger \phi_1)^2 + \{\frac{1}{2}\lambda_5(\phi_1^\dagger \phi_1)^2 + \{\lambda_6(\phi_1^\dagger \phi_1) + \\ & \lambda_7(\phi_2^\dagger \phi_2)\}(\phi_1^\dagger \phi_2) + h.c\} \quad (2) \end{aligned}$$

where,  $\phi_1, \phi_2$  are two Higgs doublets. Because of the addition of another doublet, 2HDM comprises of five physical Higgs that include CP-even neutral Higgs  $h$  and  $H$ , CP-odd neutral Higgs  $A$  and the charged Higgs  $H^\pm$ . Parameters used in the above expressions are  $m_{11}, m_{22}, \lambda_1, \lambda_2, \lambda_3, \lambda_4, m_{12}^2, \lambda_5, \lambda_6, \lambda_7$  and h.c stands for hermition conjugate. First six parameters are real and last four parameters can be both real or complex. Complex parameters violate CP which is not desirable, that's why only real case is considered here. After inserting doublets, quadratic, cubic and quartic terms are obtained. Quadratic terms give us information about masses, while cubic and quartic terms give us information about couplings. This scalar potential includes Flavor Changing Neutral Currents (FCNCs). These can be avoided by imposing  $Z_2$  symmetry i.e.  $\phi_1 \rightarrow \phi_1$ , and  $\phi_2 \rightarrow -\phi_2$  or in another term as  $\phi_1 \rightarrow -\phi_1$  and  $\phi_2 \rightarrow \phi_2$ , in Lagrangian. If potential  $Z_2$  is

symmetric then  $m_{12}^2$ ,  $\lambda_6$ ,  $\lambda_7$  are forbidden [37]. However, parameter  $m_{12}^2 \neq 0$  is considered because  $Z_2$  symmetry is softly broken by dimension two operators  $\phi_1^\dagger \phi_2$  or  $\phi_2^\dagger \phi_1$  [34]. After imposing  $Z_2$  symmetry, Higgs bosons couplings to fermions are restricted. Various Higgs boson couplings to fermions are presented in Table I. Various scenarios of Higgs boson couplings to fermions obeying  $Z_2$  symmetry table.1

<b>PType</b>	<b>Description</b>	$Q_u$	$Q_d$	$l^\pm$	<b>Detail</b>
I	Fermi-phobic	$\phi_2$	$\phi_2$	$\phi_2$	Charged fermions couple to second doublet only
II	MSSM-like	$\phi_2$	$\phi_1$	$\phi_1$	Up and down type couple to different doublets
X	Lepton- specific	$\phi_2$	$\phi_2$	$\phi_1$	Charged lepton couple to first doublets
Y	Flipped	$\phi_2$	$\phi_1$	$\phi_2$	Charged lepton couple to second doublet as flipped form type II

TABLE I: Various scenarios of Higgs boson couplings to fermions obeying  $Z_2$  symmetry

In SM, coupling of fermions ( $f$ ) with Higgs boson can be given as  $m_f/\nu$ . So Yukawa Lagrangian in physical basis is given as [38],

$$\mathcal{L}_{Yukawa}^{2HDM} = - \sum_{f=u,d,l} \frac{m_f}{\nu} \left( \xi_h^f \bar{f} f h + \xi_H^f \bar{f} f H - i \xi_A^f \bar{f} \gamma_5 f A \right) - \left\{ \frac{\sqrt{2}}{\nu} V_{ud} \bar{u} (m_u \xi_A^u P_L + m_d \xi_A^u P_R) d H^+ + \frac{\sqrt{2} m_l \xi_A^l}{\nu} \bar{\nu}_L l_R H^+ + h.c. \right\} \quad (3)$$

where  $V_{q\bar{q}}$  represents CKM matrix and  $P_{L,R} = \frac{1}{2}(1 \pm \gamma_5)$  are projection operators for left and right-handed fermions.  $\xi_h^f$ ,  $\xi_A^f$ ,  $\xi_H^f$  are coupling parameters whose values are given in Table II. Values of Yukawa coupling for Type-I of 2HDM table.2. Finally, free parameters used in this model are Higgs masses ( $m_h$ ,  $m_H$ ,  $m_A$ ,  $m_H^\pm$ ), ratio of vacuum expectation values ( $\tan \beta$ ), soft discrete symmetry breaking ( $m_{12}^2$ ) and basis independent quantities  $\sin \beta \alpha = \sin(\beta - \alpha)$ , and  $\cos \beta \alpha = \cos(\beta - \alpha)$  which are related to the CP-even neutral scalar mass eigenstate and mixing angle ( $\beta - \alpha$ ) that shows mixing between CP-even neutral Higgs states [39]. These free parameters

	$\xi_h^u$	$\xi_h^d$	$\xi_h^l$	$\xi_H^u$	$\xi_H^d$	$\xi_H^l$	$\xi_A^u$	$\xi_A^d$	$\xi_A^l$
Type-I	$\frac{\cos \alpha}{\sin \beta}$	$\frac{\cos \alpha}{\sin \beta}$	$\frac{\cos \alpha}{\sin \beta}$	$\frac{\sin \alpha}{\sin \beta}$	$\frac{\sin \alpha}{\sin \beta}$	$\frac{\sin \alpha}{\sin \beta}$	$\cot \beta$	$-\cot \beta$	$-\cot \beta$

TABLE II: Values of Yukawa coupling for Type-I of 2HDM.

need to be constrained somehow. Following constraints defined on a theoretical base in 2HDM are applied.

- **Stability:** Potential must be positive everywhere. This will provide lower bound to potential [34, 36, 40–46].
- **Unitarity:** Partial wave amplitude  $a_0$  for  $l = 0$  must be less than unity at High energies [39, 47].
- **Perturbativity:** This condition puts an upper bound on quartic couplings, according to which  $|\lambda_i| \leq 4\pi$  ( $i=1,2,\dots,7$ ) [34] for quartic coupling.

These theoretical constraints are checked for parameter space using *2HDMC\_v1.8.0*.

There is another set of constraints, inspired by the previous experiments. Experimental constraints mentioned on page 3 of ref. [46] are used for the measurement of trilinear Higgs coupling.

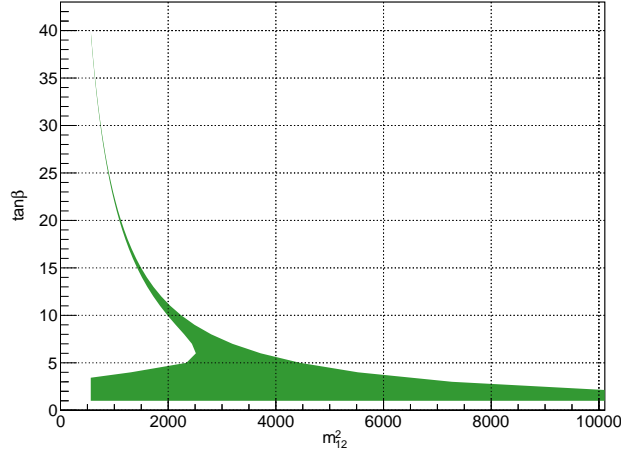


FIG. 1: Theoretical allowed region at Higgs mass 150 GeV

All computations are carried out in the exact alignment limit, i.e.  $\sin(\beta - \alpha) = 1$ , where  $h$  behaves like a SM Higgs and becomes indistinguishable from the SM Higgs boson in terms of mass and couplings. Inspired by the reference [48] and the current experimental results at the LHC [49], masses of all the extra Higgs bosons are set to be  $m_\phi = m_H^0 = m_A^0 = m_H^\pm$ . This selection also minimizes the oblique parameters [50–55], so all the electroweak observables are close to the SM ones. In the exact alignment limit, the decay of the  $H^0$  to vector boson pairs is suppressed. We performed all computations in Type-I of 2HDM. To avoid meson mixing  $\Delta M_s$  and  $B_0 \rightarrow \mu^+ \mu^-$  in Type-I, the region defined by  $2 < \tan \beta < 40$  is considered. For this scenario, theoretically allowed region is determined and then central region is considered for further analysis [37, 56–61]. One of the allowed regions is shown in Figure 1 Theoretical allowed region at Higgs mass 150 GeV figure.1.

### III. PROBING TRILINEAR HIGGS COUPLING IN 2HDM

Trilinear Higgs coupling can be probed easily in SM. Since coupling of electron and positron with Higgs  $g_{e^+e^-H}$  is very weak that's why the diagrams with Higgs as mediating particles does not contribute. Also, there is no contribution of quartic Higgs coupling  $g_{ZZHH}$ . Feynman diagrams for  $e^+e^- \rightarrow ZHH$  scattering process are given in Figure 2. All possible Feynman diagrams for the scattering process  $ZHH$  in SM. Only diagram 1 has trilinear Higgs coupling and gives significant contribution figure.2.

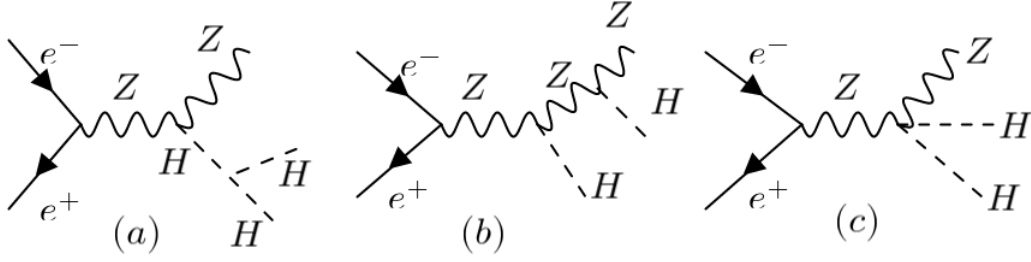


FIG. 2: All possible Feynman diagrams for the scattering process  $ZHH$  in SM. Only diagram 1 has trilinear Higgs coupling and gives significant contribution.

This case is quite challenging in 2HDM because there is not only one trilinear Higgs coupling but there are several others, which will be discussed. As exact alignment limit is used, that's why all conditions of SM also hold in 2HDM. In 2HDM, following Equations from 4equation.3.4 till 9equation.3.9 represent Higgs self-couplings as a function of  $\Lambda_i$ , where we selected two independent parameters to be  $s_{\beta\alpha} = 1$  and  $c_{\beta\alpha} = 0$  respectively. Among all the Higgs self couplings  $g_{hhH}$  vanishes, as well as, due to exact alignment limit and equal masses of all extra Higgs bosons, two other parameters  $\Lambda_6$  and  $\Lambda_7$  vanish. In addition  $g_{hHH}$  and  $g_{hAA}$  are equal and  $g_{HHH}/g_{HAA} = 3$ . Given that  $\Lambda_{345} = \Lambda_3 + \Lambda_4 + \Lambda_5$ , we can write

$$g_{h^0 h^0 h^0} = -3\nu((\Lambda_7 c_{\beta\alpha}^2 + 3\Lambda_6 s_{\beta\alpha}^2)c_{\beta\alpha} + (\Lambda_{345} c_{\beta\alpha}^2 + \Lambda_1 \delta_{\beta\alpha}^2)s_{\beta\alpha}) \Big|_{c_{\beta\alpha} \rightarrow 0} = -3\nu\Lambda_1 \quad (4)$$

$$g_{h^0 h^0 H^0} = -\nu((\Lambda_{345}(1 - 3s_{\beta\alpha}^2) + 3\Lambda_1 s_{\beta\alpha}^2)c_{\beta\alpha} + 3(\Lambda_6(2 - 3s_{\beta\alpha}^2) - \Lambda_7 c_{\beta\alpha}^2)s_{\beta\alpha}) \Big|_{c_{\beta\alpha} \rightarrow 0} = 0 \quad (5)$$

$$g_{h^0 H^0 H^0} = -\nu((3\Lambda_1 c_{\beta\alpha}^2 + \Lambda_{345}(3s_{\beta\alpha}^2 - 2))s_{\beta\alpha} + 3(\Lambda_6 + \Lambda_7 c_{\beta\alpha}^2 - 3\Lambda_6 s_{\beta\alpha}^2)c_{\beta\alpha}) \Big|_{c_{\beta\alpha} \rightarrow 0} = -\nu\Lambda_3 \quad (6)$$

$$g_{h^0 A^0 A^0} = -\nu(\Lambda_7 c_{\beta\alpha} + (\Lambda_3 + \Lambda_4 - \Lambda_5)s_{\beta\alpha}) \Big|_{c_{\beta\alpha} \rightarrow 0} = -\nu\Lambda_3 \quad (7)$$



$$g_{H^0 H^0 H^0} = -3\nu((\Lambda_1 c_{\beta\alpha}^2 + \Lambda_{345} s_{\beta\alpha}^2) c_{\beta\alpha} - \Lambda_7 s_{\beta\alpha}^2 - 3\Lambda_6 c_{\beta\alpha}^2) s_{\beta\alpha} \Big|_{c_{\beta\alpha} \rightarrow 0} = 3\nu\Lambda_7 \quad (8)$$

$$g_{H^0 A^0 A^0} = -\nu((\Lambda_3 + \Lambda_4 - \Lambda_5) c_{\beta\alpha} - \Lambda_7 s_{\beta\alpha}) \Big|_{c_{\beta\alpha} \rightarrow 0} = \nu\Lambda_7 \quad (9)$$

The measurement of Higgs self-coupling within 2HDM is difficult due to the presence of more than one Higgs. The couplings where  $h^0$ ,  $H^0$  and  $A^0$  are intermediated, do not make a noticeable contribution because of their absolute value, which is less than  $10^{-6}$ , so they can be neglected. Significant contributions are found to be from  $Z^0$  coupling only, that is why only those Feynman diagrams are taken into account in which  $Z$  boson is intermediated.

The scattering processes with various combinations of trilinear Higgs self-couplings need to be considered, i.e.,  $ZHh$ ,  $ZAh$ ,  $HHH$ ,  $hhh$ ,  $Ahh$ ,  $AAh$ ,  $AAH$ ,  $HHh$ , and  $Hhh$ . The Feynman diagrams of possible processes are shown in Figure 3. Their cross-section is less than  $10^{-11}$  pb; therefore it is not possible to detect them and they can be easily neglected. To calculate the Higgs self-coupling in two Higgs doublet model, we use the scattering processes shown in Table III. Signal processes and their corresponding couplings at Higgs mass of 150 GeV and  $\tan\beta = 10$  are shown in Table 3. These scattering processes are the only ones which can give the cross-section greater than attobarn. In Equation 5,  $g_{h^0 h^0 H^0}$  approaches zero so this coupling vanishes. The cross-section of scattering process  $e^-e^+ \rightarrow ZAA$  makes it possible to determine the coupling  $g_{h^0 A^0 A^0}$ . The coupling  $g_{h^0 H^0 H^0}$  can be determined by measuring the cross-section of process  $e^-e^+ \rightarrow ZHH$ . The cross-section of  $e^-e^+ \rightarrow Zhh$  extracts the coupling  $g_{h^0 h^0 h^0}$  which could be the same as determined in SM. The coupling  $g_{H^0 A^0 A^0}$  can be determined by two processes,  $e^-e^+ \rightarrow Ahh$  and  $e^-e^+ \rightarrow AHH$ , whereas the last mentioned process can also give  $g_{H^0 H^0 H^0}$ .

Feynman diagrams with  $Z$  as mediating particle are considered because only  $g_{e^+e^-Z}$  coupling has a major contribution. Then  $ZAA$ ,  $ZHH$ , and  $Zhh$  processes are selected for further analysis because they have reasonable cross-section [46]. The presence of trilinear Higgs coupling can be seen in Feynman diagrams for these processes given in Figure 3. Feynman diagrams involved in scattering process  $Zhh$ ,  $ZHH$  and  $ZAA$  in 2HDM are shown in Figure 3.

Measuring the cross section of  $e^+e^- \rightarrow Zhh$  will allow us to determine the coupling  $g_{Hhh}$  and  $g_{hhh}$ . The couplings  $g_{hHH}$  and  $g_{HHH}$  can be determined by analyzing  $e^+e^- \rightarrow ZHH$ . Similarly, the presence of coupling  $g_{hAA}$  and  $g_{HAA}$  can be determined by studying  $e^+e^- \rightarrow ZAA$ . In Table III, signal processes and their corresponding couplings at Higgs mass of 150 GeV and  $\tan\beta = 10$  are shown in Table 3. Trilinear Higgs self coupling which contributes to the signal processes given in first column are marked by a plus sign.

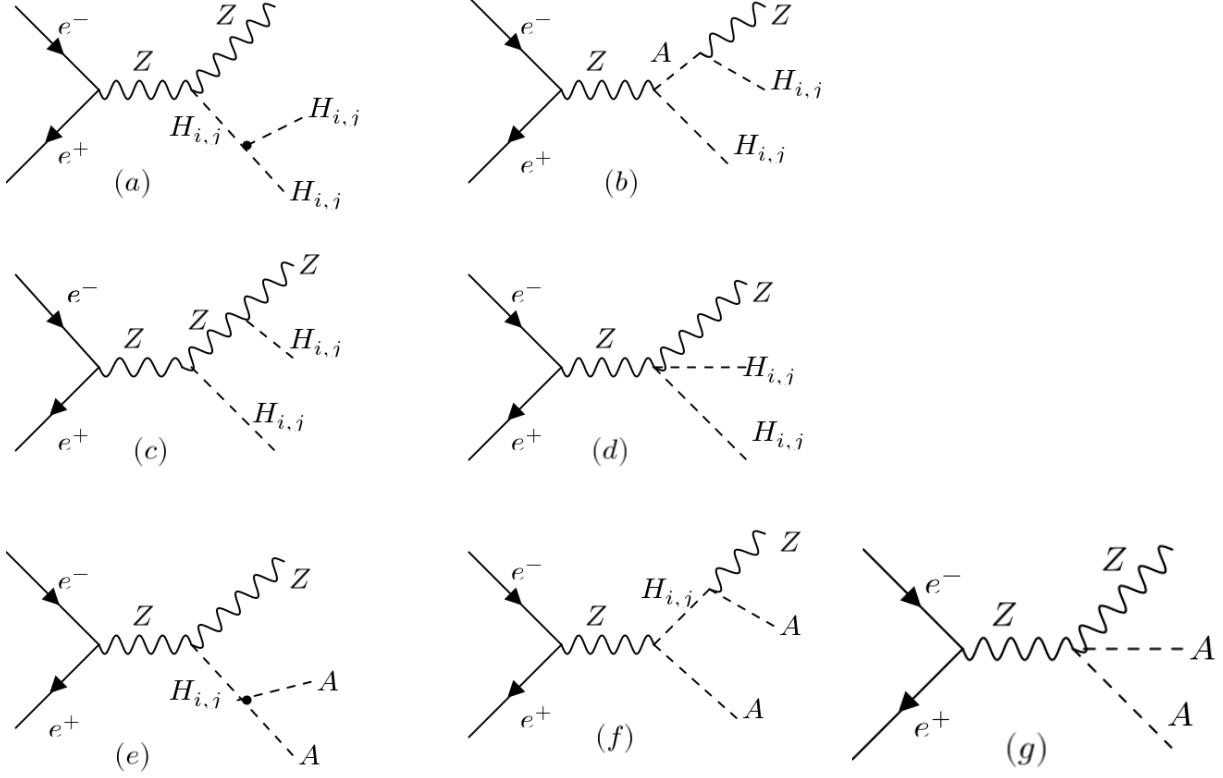


FIG. 3: Feynman diagrams involved in scattering process  $Zhh$ ,  $ZHH$  and  $ZAA$  in 2HDM.

	$g_{hHH}$	$g_{Hhh}$	$g_{hAA}$	$g_{HAA}$	$g_{hhh}$	$g_{HHH}$
$Zhh$					+	
$ZHH$	+					+
$ZAA$			+	+		

TABLE III: Signal processes and their corresponding couplings at Higgs mass of 150 GeV and  $\tan\beta = 10$

#### IV. ANALYSIS TOOLS

For the calculation of branching ratios and decay widths for selected benchmarks points within 2HDM Type-I, 2HDMC 1.8.0 is used. The theoretically allowed region is also computed for each signal scenario. Generation of events for signal as well as background is carried out through CalcHEP 3.8.5 [62] and then these events are saved in LHE file for further compilation using PYTHIA 8244[63]. Relative efficiencies at each benchmark are computed. Then HepMC 2.06.09 [64] interface is used for event record. Jet definition and reconstruction is carried out with FastJet

3.3.3 [65, 66] interface. The output is analyzed using ROOT 6.14.06 [67], which helps to draw all graphs and plots.

## V. NEUTRAL HIGGS DECAYS

Decay widths and branching ratios of different Higgs decays are calculated at  $\tan \beta = 10$  for different values of Higgs masses.

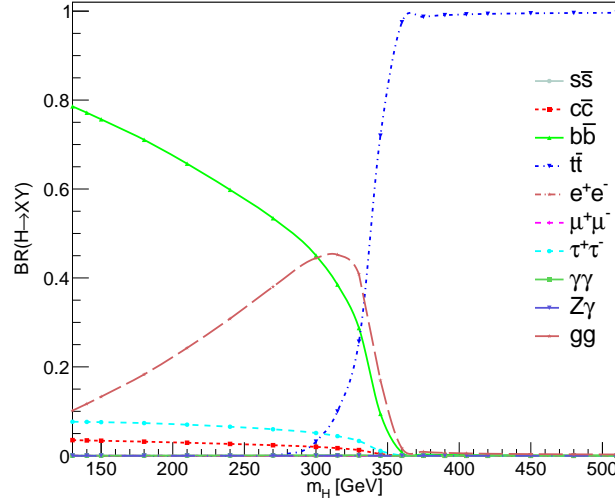


FIG. 4: Branching ratios of H decays in Type-I of 2HDM at  $\tan \beta = 10$

From Figure 4 Branching ratios of H decays in Type-I of 2HDM at  $\tan \beta = 10$  figure.4, it can be seen that prominent decay channels of  $H$  are  $b\bar{b}$  and  $t\bar{t}$ . In a mass region above 270 GeV,  $t\bar{t}$  is a prominent decay and in low mass region  $b\bar{b}$  is a prominent decay. Branching ratio of  $\tau^+\tau^-$  and  $c\bar{c}$  is quite small that is below 0.1, and for  $gg$  it increases with the increase in Higgs mass. Higgs decay branching ratios for  $\mu^+\mu^-$ ,  $s\bar{s}$ ,  $e^+e^-$ ,  $\gamma\gamma$  and  $Z\gamma$  is very small and approaches to zero. Higgs decay into  $WW$  and  $ZZ$  vanishes when  $\cos(\alpha - \beta) = 0$  is assumed.

Trilinear Higgs self coupling vertices depend upon  $\sin \alpha\beta$  and  $\cos \alpha\beta$ . And in exact alignment limit, these become independent of  $\tan \beta$ . So any value of  $\tan \beta$  can be chosen in favor of the branching ratio. To check the distribution of BR, plots are drawn between branching ratio and  $\tan \beta$  at various Higgs masses.

Figure 5 Distribution of branching ratio at various Higgs masses as a function of  $\tan \beta$  (left). Distribution of branching ratio at various Higgs masses as a function of  $m_{12}^2$  at  $\tan \beta = 9$  (right) figure.5 (left) shows that there is no significant change in BR with the change in the value of  $\tan \beta$ . It is

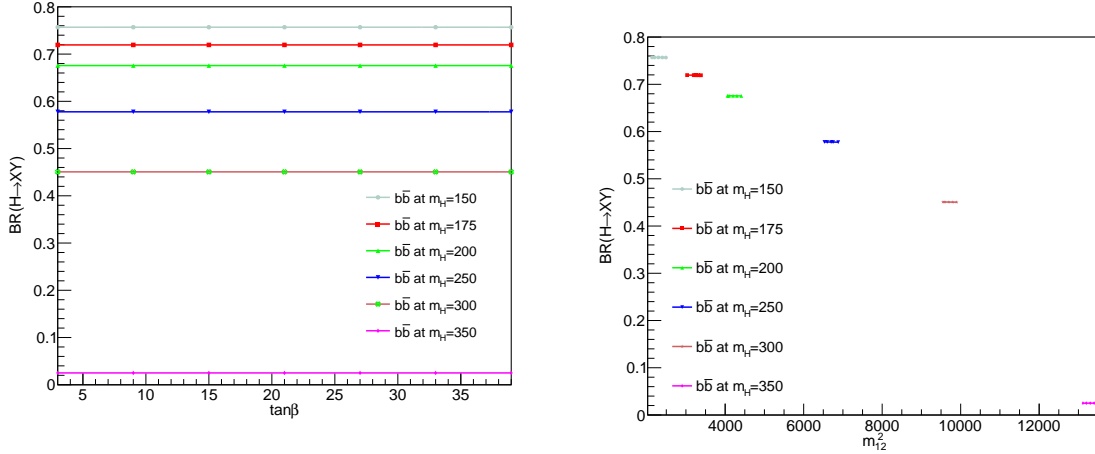


FIG. 5: Distribution of branching ratio at various Higgs masses as a function of  $\tan \beta$  (left). Distribution of branching ratio at various Higgs masses as a function of  $m_{12}^2$  at  $\tan \beta = 9$  (right).

important to check change in branching ratio with the change in the value of  $m_{12}^2$ . Figure 5 shows that value of BR changes slightly as we move towards the upper limit of the allowed region. But this change is not prominent. So, central value of theoretically allowed region and  $\tan \beta = 10$  is selected for further computations.

## VI. BENCHMARK POINTS, SIGNAL AND BACKGROUND PROCESSES

Various processes are selected as signal processes for the analysis. In all these processes double Higgs is produced along with  $Z$  boson by Higgs strahlung process generating a trilinear Higgs vertex. All these processes are generated by the annihilation of electron and positron along with  $Z$  as mediating particle at Compact Linear Collider (CLIC) at centre of mass energy  $\sqrt{s} = 1.5$  TeV. Signal processes have  $ZHH$ ,  $Zhh$ , and  $ZAA$  as decay products where  $Z$  decays into di-jets while  $H$ ,  $h$  and  $A$  decay into  $b$  quark di-jets. So, in each process, there are six jet final states comprising of two light jets and four  $b$  quark jets.

$$e^+e^- \rightarrow Z^* \rightarrow ZHH, Zhh, ZAA \rightarrow jj\bar{b}b\bar{b}b$$

After analyzing the results given in section V, different benchmark points are selected within parameter space of 2HDM which are given in Table IV. Benchmark points for different parameters

within the allowed region table.4.

	$m_h$ GeV	$m_H$ GeV	$m_A$ GeV	$m_{H^\pm}$ GeV	$m_{12}^2$	$\tan \beta$	$\sin(\beta - \alpha)$
BP1	125.09	130	130	130	1433-1688	10	1
BP2		140	140	140	1700-1956		
BP3		150	150	150	1987-2243		
BP4		175	175	175	2792-3047		
BP5		200	200	200	3720-3975		
BP6		225	225	225	4772-5027		
BP7		250	250	250	5948-6203		

TABLE IV: Benchmark points for different parameters within the allowed region.

The production cross-section of signal processes is very small, in the range of  $\cong 0.1 - 0.2 fb$  despite applying all constraints. This difficulty is further increased by the SM background. There are a number of background processes that can suppress the signal, some of which are  $t\bar{t}$ ,  $ZZ$ ,  $Zb\bar{b}$  and  $ZZZ$ . The Feynman diagrams for which are given in Figure 6 Feynman diagrams for  $t\bar{t}$ ,  $ZZ$ ,  $Zb\bar{b}$  and  $ZZZ$  backgrounds processes represented by  $p1$ ,  $p2$ ,  $p3$  and  $p4$  respectively figure.6 where  $j_s$  represent jets of  $u$ ,  $d$ ,  $s$ ,  $c$  and  $b$  quarks. It can be seen that  $Z$  bosons decay into jets resulting in 4 jets and 6 jets final state from  $ZZ$ ,  $Zb\bar{b}$  and  $ZZZ$  processes, respectively. Top quark decays into  $W$  boson and  $b$  quark, where  $W$  boson further decays into jets resulting in 6 jets final state from  $t\bar{t}$  process. For suppression of background, reconstruction of Higgs boson mass in every event will be beneficial. Because if  $b$  quark pair was not produced from neutral Higgs boson then it will not lie within the Higgs mass range and these events will be excluded.

Background processes can also be suppressed by using kinematic selection cuts. Efficiencies of background processes are given in Table V Efficiencies of SM background processes at different kinematic selection cut table.5, which shows that efficiency is maximum for  $t\bar{t}$ .

## VII. EVENT SELECTION PROCEDURE

In this section the selection criteria for events is discussed briefly. A large statistics of both signal and possible background processes are produced in the form of LHE format and then compiled by PYTHIA for Hadronization purpose by Parton fragmentation process. Many kinematical selection cuts are applied to suppress background and keep the signal process dominant. The kinematic

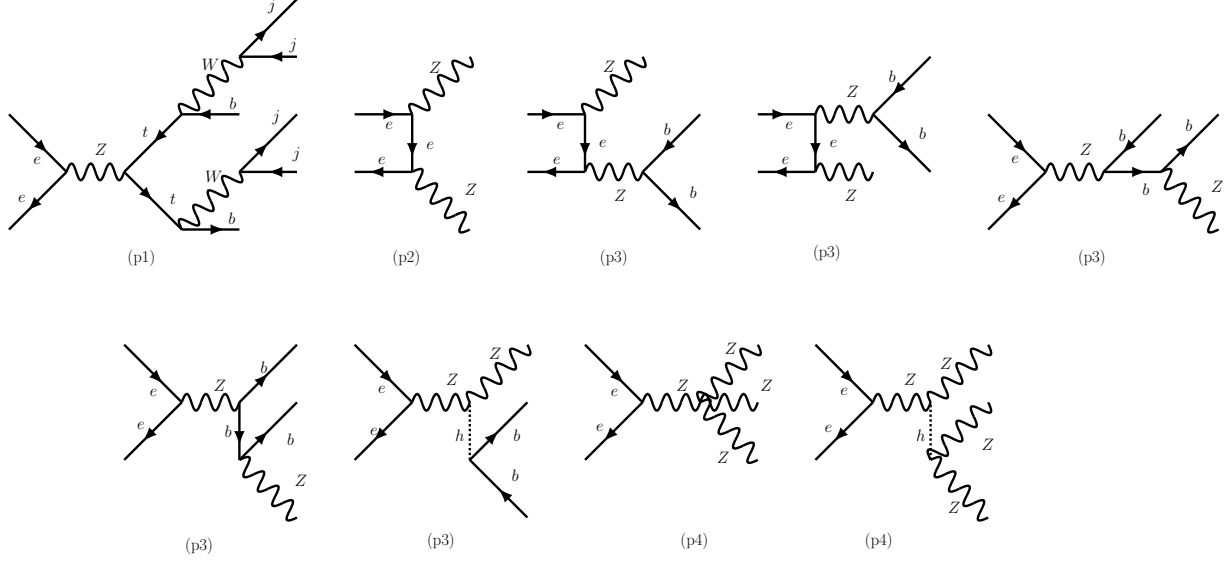


FIG. 6: Feynman diagrams for  $t\bar{t}$ ,  $ZZ$ ,  $Zb\bar{b}$  and  $ZZZ$  background processes represented by  $p1$ ,  $p2$ ,  $p3$  and  $p4$  respectively.

	$t\bar{t}$	$ZZ$	$Zb\bar{b}$	$ZZZ$
$\sigma$ [fb]	80.44	84.29	32.82	0.739
$N_{jets} \geq 5$	0.823	0.079	0.090	0.814
$N_{bjets} \geq 3$	0.327	0.009	0.230	0.016
$N_{bb} \geq 1$	0.184	0.148	0.202	0.116
<b>Total Efficiency</b>	<b>0.049</b>	<b>0.000</b>	<b>0.004</b>	<b>0.002</b>
Six jets final state	0.000	0.000	0.004	0.002

TABLE V: Efficiencies of SM background processes at different kinematic selection cuts.

variables studied to define the selection criteria include transverse momentum ( $p_T$ ), pseudo-rapidity ( $\eta$ ), azimuthal angle ( $\phi$ ), jet multiplicity ( $N_{jet}$ ), b-jet multiplicity ( $N_{b-jet}$ ),  $\Delta R$  (Jet cone size) and invariant mass ( $m_{bb}$ ).

The first step of analysis requires, writing of a simulation code in C++ and linking the libraries of simulation packages to it. After the initialization of the LHE file, desired decays are allowed. A particle loop is applied to identify the signal process. All this information is then stored in an event file. This event record is provided as an input to FastJet. In this mechanism, some of the jets lie beyond the cone size due to many factors such as the detector's impairment, magnetic field, and material influence. All the jets are sorted out by a built-in class of PYTHIA in order of highest to

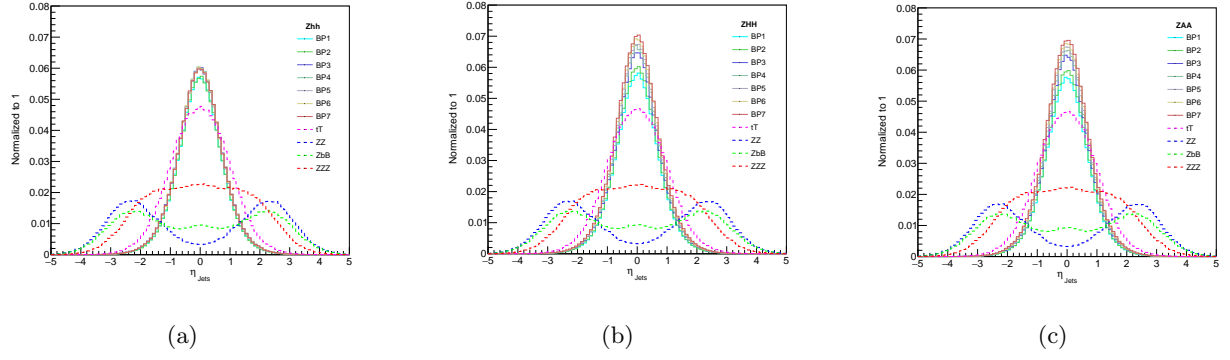


FIG. 7: Pseudorapidity distributions of jets for signal and background processes.

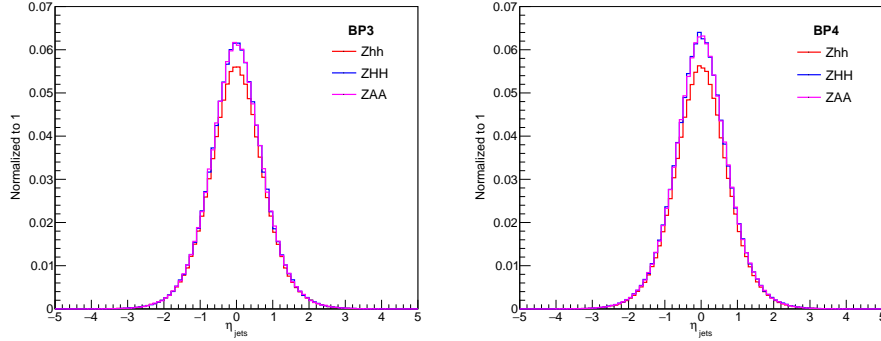


FIG. 8: Comparison of pseudorapidity distributions of various signal process.

lowest transverse momentum  $P_T^{jet}$ . First of all, a loop on sorted jets is applied and then resulting jets are passed through kinematic selection cuts.

$$P_T^{jet} \leq 10 \text{ GeV} \quad \text{and} \quad |\eta_{jet}| \leq 3 \quad (10)$$

Where,  $\eta \equiv -\ln[\tan(\theta/2)]$  is the angle between the particle and beam axis and  $\theta$  is the angle between three components of momentum and positive beam axis. Figures 7Pseudorapidity distributions of jets for signal and background processesfigure.7 and 8Comparison of pseudorapidity distributions of various signal processfigure.8 show the distribution of pseudorapidity for signal and background processes.

Particles with  $\eta = 0$  are perpendicular to the beam axis and particles having higher  $\eta$  values are lost that is why the condition given in Equation 11equation.7.11 is applied to find events with true particles. This condition will also exclude background events with high pseudorapidity values. Further cuts are applied on the resulting good jets. As six jets final state is the main feature of

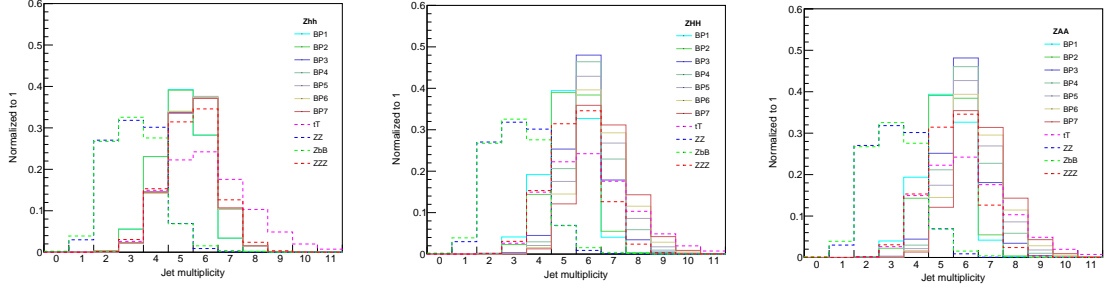


FIG. 9: Number of jets for signal and background processes.

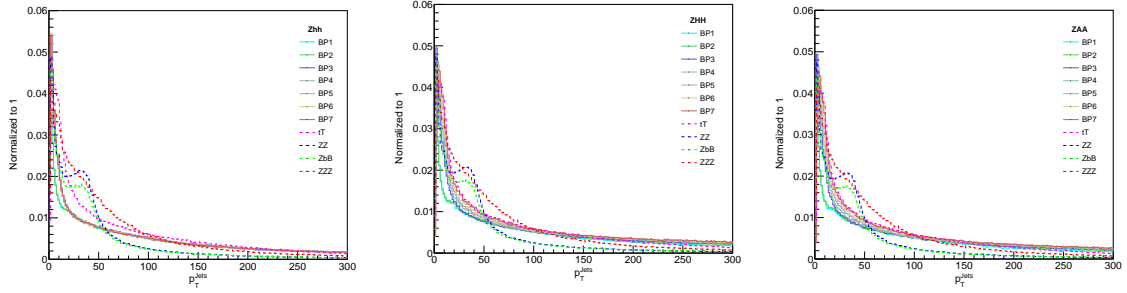


FIG. 10: Transverse momentum of jets for signal and background processes.

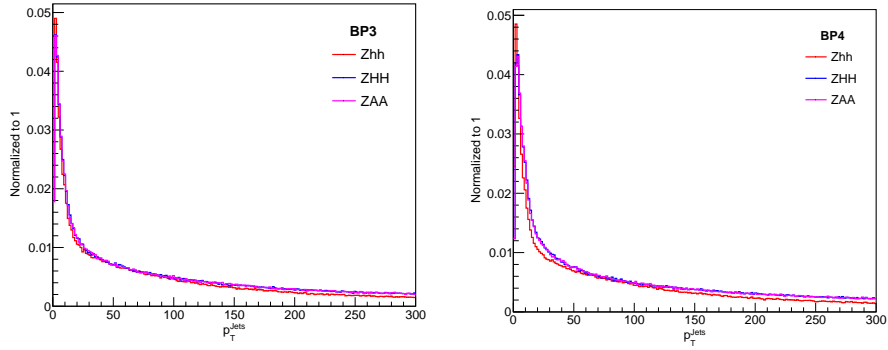


FIG. 11: Comparison of transverse momentum of jets produced in various signal process.

the signal process, another requirement is imposed to fulfill this condition,

$$N_{jets} \geq 5 \quad (11)$$

where  $N_{jets}$  is the number of jets. The number of jets produced in each event are plotted as jet multiplicity which is shown in Figure 9. Number of jets for signal and background processes is shown in Figure 9. In Figures 10 and 11, Transverse momentum of jets for signal and background processes is shown. Figure 10 and 11 show the comparison of transverse momentum of jets produced in various signal processes.



parison of transverse momentum of jets produced in various signal processesfigure.11, distribution of transverse momentum of jets for signal and background processes, and their comparison in case of different signal processes is given. Now a particle loop is applied on the list of sorted jets to identify the jets produced from  $Z$  boson decay. Then angular separation  $\Delta R$  of jets with respect to quarks is calculated. Jets with  $\Delta R < 0.4$ ,  $P_{jet}^T \geq 10 \text{ GeV}$  and  $|\eta_{jet}| \leq 3.0$  are named as light jets. The light jets are compared amongst themselves and two of them with maximum transverse momentum are selected.

The next step is the identification of b-jets from the list of sorted jets. The identification of b-jets is carried out through b-tagging where only bottom and charm quarks are allowed to pass the selection criteria. Then  $\Delta R$  between jets and bottom or charm quark is computed. In Figure 12  $\Delta R$  of b-jets for signal and background processesfigure.12,  $\Delta R$  distribution of selected jets is given for signal and background processes. Jets with  $\Delta R < 0.4$ ,  $P_{jet}^T \geq 20 \text{ GeV}$  and  $|\eta_{bjet}| \leq 3.0$  are tagged as b-jets. The resulting number of b-jets are plotted as b-jet multiplicity, shown in Figure ???. The possibility of b-jets arising from b-quark is taken to be 60% and from c-quark is taken as 10%. These values are considered as b-tagging efficiencies.

As each scattering process in the analysis contains two Higgs and each one of them decays into a b-quark pair, that is why four b-quarks must be present in the final state. This condition is attained by applying a b-jet selection cut,

$$N_{b-jets} \geq 3 \quad (12)$$

where  $N_{b-jets}$  represents the numbers of b-jets. The b-jets resulting from the above condition are then analyzed and true b-jet pairs are found, which are produced from Higgs boson decays.

## VIII. RECONSTRUCTION OF INVARIANT MASSES

In particle physics, invariant mass of a particle is defined as its mass in rest frame and given as,

$$(m_0 c)^2 = \left(\frac{E}{c}\right)^2 - |p|^2 \quad (13)$$

Using natural units, set  $c = 1$ ,

$$(m_0)^2 = (E)^2 - |p|^2 \quad (14)$$

After the selection of desired events from randomly generated events, the next step is the reconstruction of invariant masses of parent particle from its decay products. As a first step, the

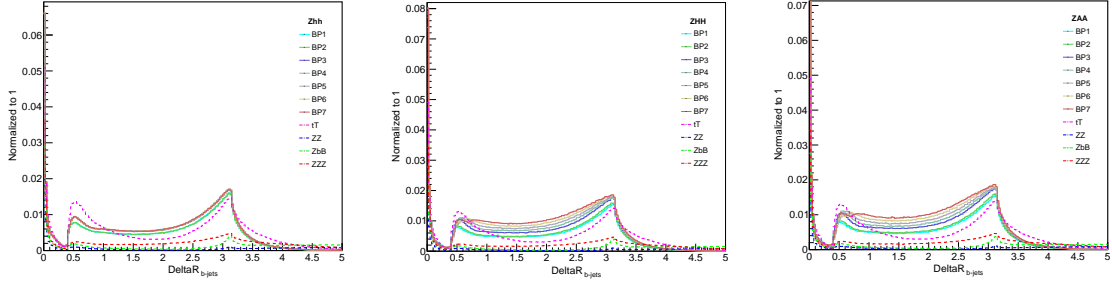


FIG. 12:  $\Delta R$  of b-jets for signal and background processes.

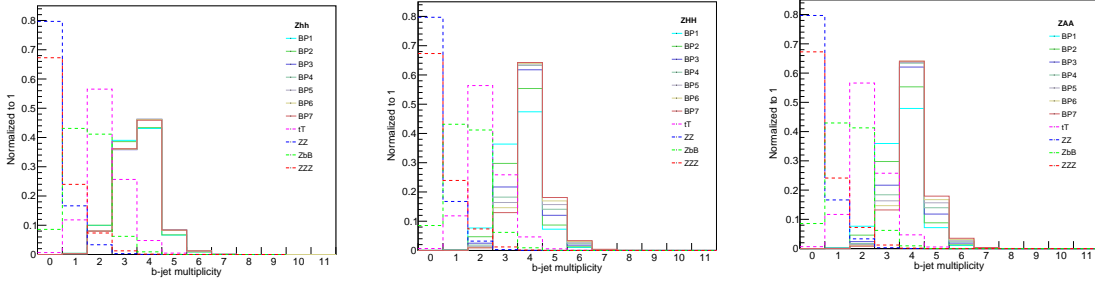


FIG. 13: No of b-jets for signal and backgrounds processes.

invariant mass of neutral Higgs is reconstructed. Events with at least four b-jets are selected and invariant mass is reconstructed for all possible b-jet pairs using the following relation,

$$m_{b_1 b_2} = \sqrt{(E_{b_1} + E_{b_2})^2 - (p_{x_{b_1}} + p_{x_{b_2}})^2 - (p_{y_{b_1}} + p_{y_{b_2}})^2 - (p_{z_{b_1}} + p_{z_{b_2}})^2} \quad (15)$$

Then difference of invariant mass  $|m_{b_1 b_2} - m_{b_3 b_4}|$  is calculated for each and every combination. The b-jet pairs with least mass difference are selected as true b-jet pairs provided they fulfill the condition,

$$N_{b\bar{b}} \geq 1 \quad (16)$$

Where,  $N_{b\bar{b}}$  is the number of true b-jet pairs. Next invariant mass of  $Z$  boson is reconstructed using the remaining jets that do not take part in Higgs boson mass reconstruction.

The invariant mass distributions for neutral Higgs bosons, shown in Figure 14 Reconstructed masses of neutral Higgs bosons from b-quark pairs produced from signal and background processes figure.14 are obtained from selected  $b\bar{b}$  combinations from events remaining after passing through many selection and kinematic cuts, that were generated at center of mass energy of 1.5

	Benchmarks	$m_{Gen.}$ [GeV]	$m_{Rec.}$ [GeV]	$m_{Corr.rec.}$ [GeV]		Benchmarks	$m_{Gen.}$ [GeV]	$m_{Rec.}$ [GeV]	$m_{Corr.rec.}$ [GeV]		Benchmarks	$m_{Gen.}$ [GeV]	$m_{Rec.}$ [GeV]	$m_{Corr.rec.}$ [GeV]
h	BP1	125.09	119.4 $\pm$ 0.101	125.5 $\pm$ 0.222	H	BP1	130	123.5 $\pm$ 0.163	131.5 $\pm$ 0.354	A	BP1	130	123.8 $\pm$ 0.160	131.8 $\pm$ 0.356
	BP2		119.0 $\pm$ 0.111	125.1 $\pm$ 0.212		BP2	140	133.8 $\pm$ 0.127	141.8 $\pm$ 0.318		BP2	140	134.1 $\pm$ 0.111	142.1 $\pm$ 0.307
	BP3		119.0 $\pm$ 0.136	125.1 $\pm$ 0.237		BP3	150	143.3 $\pm$ 0.140	151.3 $\pm$ 0.331		BP3	150	143.4 $\pm$ 0.149	151.4 $\pm$ 0.345
	BP4		118.9 $\pm$ 0.116	125.0 $\pm$ 0.217		BP4	175	167.5 $\pm$ 0.162	175.5 $\pm$ 0.353		BP4	175	167.1 $\pm$ 0.222	175.1 $\pm$ 0.418
	BP5		119.1 $\pm$ 0.145	125.2 $\pm$ 0.246		BP5	200	189.9 $\pm$ 0.271	197.9 $\pm$ 0.462		BP5	200	191.9 $\pm$ 0.201	199.9 $\pm$ 0.397
	BP6		118.8 $\pm$ 0.111	124.9 $\pm$ 0.212		BP6	250	240.2 $\pm$ 0.236	248.2 $\pm$ 0.427		BP6	225	214.7 $\pm$ 0.275	222.7 $\pm$ 0.471
	BP7		118.6 $\pm$ 0.126	124.7 $\pm$ 0.227		BP7	250	240.2 $\pm$ 0.236	248.2 $\pm$ 0.427		BP7	250	238.8 $\pm$ 0.257	246.8 $\pm$ 0.453

TABLE VI: The generated ( $m_{Gen.}$ ), reconstructed ( $m_{rec.}$ ) and corrected reconstructed ( $m_{Corr.rec.}$ ) Higgs masses along with relative uncertainties at  $\sqrt{s} = 1.5$  TeV.

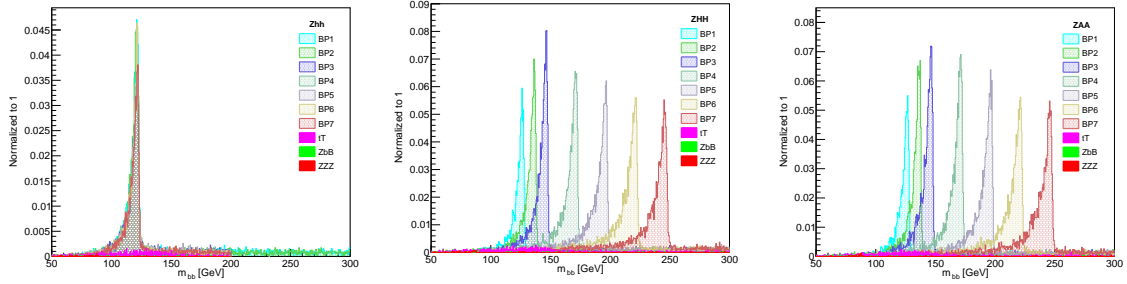


FIG. 14: Reconstructed masses of neutral Higgs bosons from b-quark pairs produced from signal and background processes.

TeV. The contribution of signal, as well as background, is also shown. It can be seen that there is some contribution of SM backgrounds  $t\bar{t}$ ,  $ZZ$ , and  $ZZZ$ . Contribution of  $t\bar{t}$  background is prominent but under control. All other backgrounds appear below the signal.

All distributions are normalized on the basis of  $L \times \sigma \times \epsilon$ , where  $L$  is the integrated luminosity,  $\sigma$  represents the total cross-section and  $\epsilon$  represents the total efficiency. Calculations are performed for two values of integrated luminosity i.e.  $1000 \text{ fb}^{-1}$  and  $2500 \text{ fb}^{-1}$ . The  $\sigma \times BR$  is obtained by multiplying cross-section values in Table VII Efficiencies of signal processes  $Zhh$ ,  $ZHH$  and  $ZAA$  at different kinematic and selection cut table.7 with the corresponding branching ratios of decay products,  $Z \rightarrow jj$  and  $H \rightarrow b\bar{b}$ . The selection efficiencies of Higgs mass distributions are calculated by dividing the number of events used for reconstruction of Higgs mass by the total number of events generated. Fit functions are applied on the obtained Higgs mass distributions. A Gaussian function is used to fit these distributions, where the Mean parameter represents the fitted value of Higgs mass. It gives the value at the center of the peak of the distribution. Values obtained from Mean are named as reconstructed mass ( $m_{Rec.}$ ). Generated mass ( $m_{Gen.}$ ) of Higgs

are also given for contrast. It can be seen from Table VI The generated ( $m_{Gen.}$ ), reconstructed ( $m_{rec.}$ ) and corrected reconstructed ( $m_{Corr.rec.}$ ) Higgs masses along with relative uncertainties at  $\sqrt{s} = 1.5$  TeV table.6 that there is a difference between generated and reconstructed masses. These variations may be caused due to different sources such as unreliability arising from jet clustering algorithm or wrong jet identification, jet tagging efficiency, selection of the fit function, fitting method, and inaccuracy in the measured energy and momentum of the particles. These errors can be resolved by improving the jet clustering algorithm, b-tagging efficiency, and fitting method. However, these improvements are out of the purviews of this study. A simple offset correction is implemented in this study to minimize errors. This off-set correction is tried as follows. It can be seen from Table VI The generated ( $m_{Gen.}$ ), reconstructed ( $m_{rec.}$ ) and corrected reconstructed ( $m_{Corr.rec.}$ ) Higgs masses along with relative uncertainties at  $\sqrt{s} = 1.5$  TeV table.6 that, on average, values of reconstructed masses of  $h$ ,  $H$ , and  $A$  are approximately 6.12, 8.04, and 8.03 lower than generated masses respectively. To remove this error, same values are added to the reconstructed masses and values thus obtained are named as corrected reconstructed mass ( $m_{Corr.rec.}$ ). It can be seen from the Table VI The generated ( $m_{Gen.}$ ), reconstructed ( $m_{rec.}$ ) and corrected reconstructed ( $m_{Corr.rec.}$ ) Higgs masses along with relative uncertainties at  $\sqrt{s} = 1.5$  TeV table.6 that corrected reconstructed masses are in accordance with generated masses. Hence it can be deduced that signal candidate masses are observable at these benchmarks points.

## IX. EVENT SELECTION EFFICIENCIES

In this study, 85000 events are generated and compiled for signal processes to get a better result from simulation for selected benchmarks points. The signal efficiency corresponding to each selection cut is then computed and at the end, total efficiency for all cuts is calculated. The efficiency obtained at the end of the whole simulation process corresponds to six jet final state which comprises of two light jets coming from Z boson decays and four b-jets coming from decays of Higgs boson. All these efficiencies mentioned in Table VII Efficiencies of signal processes  $Zhh$ ,  $ZHH$  and  $ZAA$  at different kinematic and selection cut table.7, are calculated at the center of mass energy of 1.5 TeV. It can be seen from Table VII Efficiencies of signal processes  $Zhh$ ,  $ZHH$  and  $ZAA$  at different kinematic and selection cut table.7 that signal processes have significant efficiencies at all benchmark points for selected BPs. Mostly six jets are present in generated events of signal processes. This is happening because of  $H \rightarrow b\bar{b}$  and  $Z \rightarrow jj$

	BP1	BP2	BP3	BP4	BP5	BP6	BP7
Process $\rightarrow Zh\bar{h}$							
$\sigma$ [fb]	0.207	0.207	0.207	0.207	0.207	0.207	0.207
$N_{jets} \geq 5$	0.710	0.710	0.832	0.832	0.833	0.835	0.831
$N_{bjets} \geq 3$	0.970	0.967	0.957	0.957	0.957	0.956	0.957
$N_{bb} \geq 1$	0.683	0.688	0.676	0.674	0.673	0.672	0.672
<b>Total Efficiency</b>	<b>0.470</b>	<b>0.472</b>	<b>0.538</b>	<b>0.537</b>	<b>0.537</b>	<b>0.536</b>	<b>0.535</b>
Six jets final state	0.469	0.471	0.538	0.536	0.536	0.535	0.534
Expected Events at $1000\text{ fb}^{-1}$	83	83	95	95	95	94	94
Expected Events at $2500\text{ fb}^{-1}$	207	208	237	236	236	236	236
Process $\rightarrow ZHH$							
$\sigma$ [fb]	0.162	0.156	0.150	0.136	0.123	0.110	0.098
$N_{jets} \geq 5$	0.765	0.832	0.952	0.969	0.979	0.984	0.987
$N_{bjets} \geq 3$	0.971	0.978	0.980	0.984	0.987	0.990	0.992
$N_{bb} \geq 1$	0.704	0.760	0.797	0.825	0.841	0.858	0.874
<b>Total Efficiency</b>	<b>0.523</b>	<b>0.619</b>	<b>0.743</b>	<b>0.787</b>	<b>0.812</b>	<b>0.836</b>	<b>0.855</b>
Six jets final state	0.523	0.616	0.741	0.784	0.810	0.833	0.852
Expected Events at $1000\text{ fb}^{-1}$	92	103	117	107	93	80	67
Expected Events at $2500\text{ fb}^{-1}$	230	258	292	267	233	200	168
Process $\rightarrow ZAA$							
$\sigma$ [fb]	0.162	0.156	0.150	0.136	0.123	0.110	0.098
$N_{jets} \geq 5$	0.764	0.834	0.953	0.969	0.978	0.983	0.987
$N_{bjets} \geq 3$	0.972	0.979	0.980	0.985	0.987	0.990	0.992
$N_{bb} \geq 1$	0.709	0.759	0.796	0.824	0.842	0.858	0.872
<b>Total Efficiency</b>	<b>0.527</b>	<b>0.619</b>	<b>0.744</b>	<b>0.787</b>	<b>0.813</b>	<b>0.835</b>	<b>0.853</b>
Six jets final state	0.525	0.617	0.742	0.784	0.811	0.832	0.850
Expected Events at $1000\text{ fb}^{-1}$	77	84	93	80	66	53	41
Expected Events at $2500\text{ fb}^{-1}$	192	210	233	201	165	132	101

TABLE VII: Efficiencies of signal processes  $Zhh$ ,  $ZHH$  and  $ZAA$  at different kinematic and selection cuts.

decays, where two jets are coming from  $Z$  decay and four jets are coming from double Higgs decays. The efficiency of jets production (efficiency is detector parameter while production is accelerator parameter, both are unrelated) increases with the increase in neutral Higgs boson mass.

	BP1	BP2	BP3	BP4	BP5	BP6	BP7		BP1	BP2	BP3	BP4	BP5	BP6	BP7
Process $\rightarrow Zh\bar{h}$															
$\mathcal{L}_{int.} [fb^{-1}]$	1000							$\mathcal{L}_{int.} [fb^{-1}]$	2500						
$S$	42.1	44.3	764.8	762.3	679.7	771.0	765.9	$S$	99.4	104.7	1753.4	1750.1	1699.3	1713.8	1727.4
$B$	1755.6	1755.6	64508.8	64508.8	58205.9	65781.9	64913.6	$B$	2218.1	2218.1	145515.0	145515.0	145515.0	145515.0	145515.0
$S/B$	0.02	0.03	0.01	0.01	0.01	0.01	0.01	$S/B$	0.04	0.05	0.01	0.01	0.01	0.01	0.01
$S/\sqrt{B}$	1.01	1.06	3.01	3.00	2.82	3.01	3.01	$S/\sqrt{B}$	2.11	2.22	4.60	4.59	4.45	4.49	4.53
$\epsilon_{Total}$	0.24	0.25	4.34	4.33	3.86	4.38	4.35	$\epsilon_{Total}$	0.23	0.24	3.98	3.97	3.86	3.89	3.92
Process $\rightarrow ZHH$															
$\mathcal{L}_{int.} [fb^{-1}]$	1000							$\mathcal{L}_{int.} [fb^{-1}]$	2500						
$S$	56.4	75.8	36.0	53.5	52.9	35.7	35.2	$S$	137.5	153.8	162.8	136.4	107.4	85.5	68.3
$B$	2942.0	5684.9	1246.4	308.2	294.7	300.3	287.1	$B$	4159.6	4802.6	2867.4	1105.2	669.7	442.4	475.9
$S/B$	0.02	0.013	0.03	0.17	0.18	0.12	0.12	$S/B$	0.03	0.03	0.06	0.12	0.16	0.19	0.14
$S/\sqrt{B}$	1.04	1.00	1.02	3.05	3.08	2.02	2.08	$S/\sqrt{B}$	2.13	2.22	3.04	4.10	4.15	4.07	3.13
$\epsilon_{Total}$	0.32	0.45	0.23	0.40	0.46	0.37	0.45	$\epsilon_{Total}$	0.13	0.37	0.41	0.40	0.37	0.36	0.35
Process $\rightarrow ZAA$															
$\mathcal{L}_{int.} [fb^{-1}]$	1000							$\mathcal{L}_{int.} [fb^{-1}]$	2500						
$S$	44.1	50.5	27.0	41.0	30.3	28.6	20.7	$S$	61.9	123.3	133.3	101.2	75.7	72.9	42.7
$B$	1339.3	2284.4	726.7	344.4	228.0	187.5	344.5	$B$	3063.2	3318.3	4244.8	605.7	570.1	581.7	1798.9
$S/B$	0.03	0.02	0.04	0.12	0.13	0.15	0.06	$S/B$	0.02	0.04	0.03	0.17	0.13	0.13	0.02
$S/\sqrt{B}$	1.20	1.06	1.00	2.21	2.01	2.08	1.12	$S/\sqrt{B}$	1.12	2.14	2.05	4.11	3.17	3.02	1.00
$\epsilon_{Total}$	0.30	0.37	0.22	0.40	0.37	0.45	0.44	$\epsilon_{Total}$	0.17	0.36	0.43	0.40	0.37	0.46	0.36

TABLE VIII: Values of total signal efficiency  $\epsilon_{Total}$ , signal and background events, signal significance, signal to background ratio for processes  $Zhh$ ,  $ZHH$  and  $ZAA$  for integrated luminosities of  $1000 fb^{-1}$  and  $2500 fb^{-1}$  at  $\sqrt{s} = 1.5$  TeV.

## X. SIGNAL SIGNIFICANCE

To check the visibility of the neutral Higgs boson at Compact Linear Collider for selected benchmarks, the signal significance is computed for each neutral Higgs mass distribution by incorporating total number of signal and background events of neutral Higgs bosons within selected mass limit. Signal significance is computed for the two integrated luminosities i.e.  $1000 fb^{-1}$  and  $2500 fb^{-1}$ . The computation results including signal  $S$  and background  $B$ , signal to background ratio  $S/B$ , signal significance  $S/\sqrt{B}$  and total efficiency  $\epsilon$  at  $\sqrt{s} = 1.5$  TeV are given in Table VIII. To be specific, for  $h$  it can be seen from Table VIII Values of total signal efficiency  $\epsilon_{Total}$ , signal and background events, signal significance, signal to background ratio for processes  $Zhh$ ,  $ZHH$  and  $ZAA$  for integrated luminosities of  $1000 fb^{-1}$  and  $2500 fb^{-1}$  at  $\sqrt{s} = 1.5$  TeV table.8 that it is observable at  $m_h = 125$  GeV and  $150 \leq m_H \leq 250$  GeV for both  $1000 fb^{-1}$  and  $2500 fb^{-1}$  integrated luminosity. Also from Table VIII Values of total signal

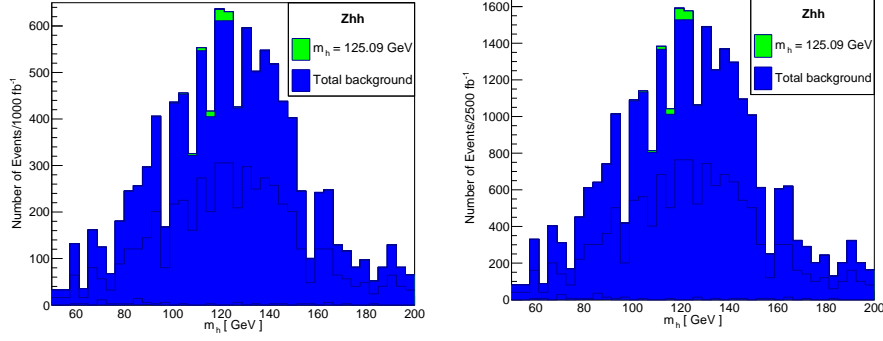


FIG. 15: Light Higgs mass distribution of  $h$  at integrated luminosity  $1000 \text{ fb}^{-1}$  (left) and  $2500 \text{ fb}^{-1}$  (right) at  $\sqrt{s} = 1.5 \text{ TeV}$ .

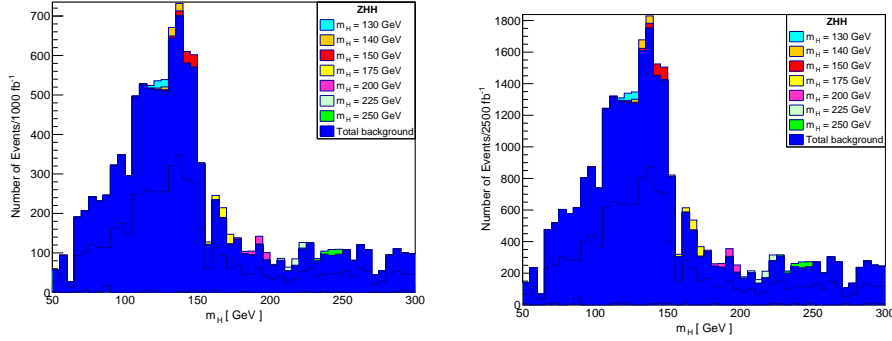


FIG. 16: Heavy Higgs mass distribution of  $H$  at integrated luminosity  $1000 \text{ fb}^{-1}$  (left) and  $2500 \text{ fb}^{-1}$  (right) at  $\sqrt{s} = 1.5 \text{ TeV}$ .

efficiency  $\epsilon_{Total}$ , signal and background events, signal significance, signal to background ratio for processes  $Zhh$ ,  $ZHH$  and  $ZAA$  for integrated luminosities of  $1000 \text{ fb}^{-1}$  and  $2500 \text{ fb}^{-1}$  at  $\sqrt{s} = 1.5 \text{ TeV}$  table.8, we can deduce that  $H$  is observable at  $175 \leq m_H \leq 250 \text{ GeV}$  for integrated luminosity of  $1000 \text{ fb}^{-1}$  and at  $130 \leq m_H \leq 250 \text{ GeV}$  for integrated luminosity of  $2500 \text{ fb}^{-1}$ . The Table VIII Values of total signal efficiency  $\epsilon_{Total}$ , signal and background events, signal significance, signal to background ratio for processes  $Zhh$ ,  $ZHH$  and  $ZAA$  for integrated luminosities of  $1000 \text{ fb}^{-1}$  and  $2500 \text{ fb}^{-1}$  at  $\sqrt{s} = 1.5 \text{ TeV}$  table.8 shows that  $A$  is observable at  $m_A = 175 \text{ GeV}$  for integrated luminosity of  $1000 \text{ fb}^{-1}$  and at  $150 \leq m_A \leq 225 \text{ GeV}$  for integrated luminosity of  $2500 \text{ fb}^{-1}$ . Signal to background candidate mass distributions are shown in Figures 15 Light Higgs mass distribution of  $h$  at integrated luminosity  $1000 \text{ fb}^{-1}$  (left) and  $2500 \text{ fb}^{-1}$  (right) at  $\sqrt{s} = 1.5 \text{ TeV}$  figure.15, 16 Heavy Higgs mass distribution of  $H$  at integrated luminosity  $1000 \text{ fb}^{-1}$  (left) and  $2500 \text{ fb}^{-1}$  (right) at  $\sqrt{s} = 1.5 \text{ TeV}$  figure.16 and 17 Pseudo-scalar Higgs mass distribution of

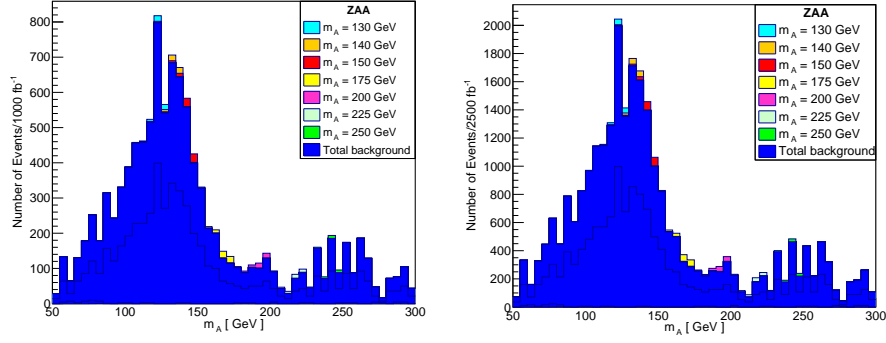


FIG. 17: Pseudo-scalar Higgs mass distribution of  $A$  at integrated luminosity  $1000 \text{ fb}^{-1}$  (left) and  $2500 \text{ fb}^{-1}$  (right) at  $\sqrt{s} = 1.5 \text{ TeV}$ .

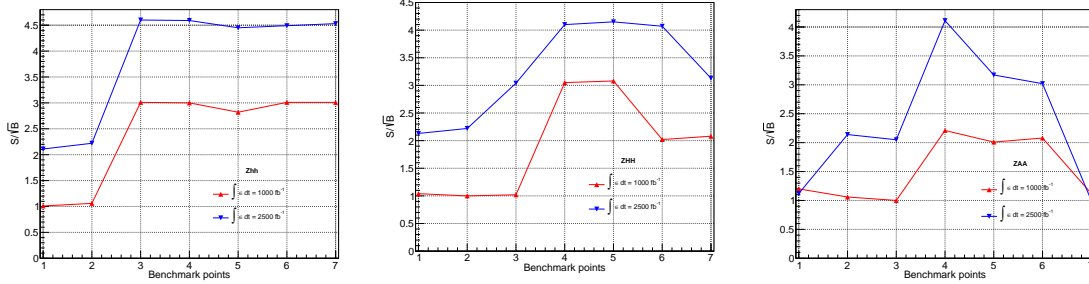


FIG. 18: Behavior of signal significance for processes  $Zhh$ ,  $ZHH$  and  $ZAA$  respectively for each benchmark point at integrated luminosity  $1000 \text{ fb}^{-1}$  and  $2500 \text{ fb}^{-1}$ .

$A$  at integrated luminosity  $1000 \text{ fb}^{-1}$  (left) and  $2500 \text{ fb}^{-1}$  (right) at  $\sqrt{s} = 1.5 \text{ TeV}$  figure.17 for integrated luminosity of 1000 and  $2500 \text{ fb}^{-1}$  at  $\sqrt{s} = 1.5 \text{ TeV}$ .

The Figure 18 Behavior of signal significance for processes  $Zhh$ ,  $ZHH$  and  $ZAA$  respectively for each benchmark point at integrated luminosity  $1000 \text{ fb}^{-1}$  and  $2500 \text{ fb}^{-1}$  figure.18 shows variation in signal significance with each benchmark point at an integrated luminosity of  $1000 \text{ fb}^{-1}$  and  $2500 \text{ fb}^{-1}$  for signal processes  $Zhh$ ,  $ZHH$  and  $ZAA$  respectively. It can be seen that with the increase in integrated luminosity, the signal significance also increases. Signal significance increases up to BP3 then it remains almost constant for the process  $Zhh$  and increases up to BP4 for the o processes  $ZHH$  and  $ZAA$ , and then decreases for higher BPs.



## XI. CONCLUSION

This study is carried out within Type-I of 2HDM in standard model like scenario. Different benchmark points are selected in the parameter space of 2HDM. Observability of standard model Higgs  $h$ , CP-even heavy Higgs  $H$ , and pseudoscalar Higgs  $A$  is evaluated. Three signal processes  $e^+e^- \rightarrow Zhh \rightarrow jj\bar{b}\bar{b}\bar{b}\bar{b}$ ,  $e^+e^- \rightarrow ZHH \rightarrow jj\bar{b}\bar{b}\bar{b}\bar{b}$  and  $e^+e^- \rightarrow Zhh \rightarrow jj\bar{b}\bar{b}\bar{b}\bar{b}$  are selected for analysis. Left-right-handed polarized incoming beams are used to enhance signal cross-section. Vertices involved in these processes depend upon  $\sin(\beta - \alpha)$  that is why in exact alignment and equal Higgs masses regime, trilinear Higgs vertices become simplified and these processes become independent of  $\tan\beta$ . So lower value of  $\tan\beta$  can be taken in support of  $h, H, A \rightarrow b\bar{b}$  decay without leaving any destructive effects on  $Zhh, ZHH$  and  $ZAA$  production. Also in this study hadronic decay of  $Z$  boson is taken that can cause many errors and uncertainties due to mistagging and jet misidentification but this prominent decay channel will compensate for these errors and uncertainties. Various benchmark points are taken at the center of mass-energy of 1.5 TeV for CLIC and event generation is carried out at each point separately. Simulation results show that the proposed analysis can be used to observe signal scenarios considered in this study because candidate mass distributions have excess of events on the top of backgrounds. Fitting functions applied on the candidate mass distributions show that the corrected reconstructed masses are very close to the generated ones. The signal significance for all signal scenarios is calculated for integrated luminosity of 1000 and 2500  $fb^{-1}$ . Computation results show that there are a fewer numbers of events at integrated luminosity of 1000  $fb^{-1}$ , due to less scattering cross-section (or production cross-section) over total backgrounds and increases up to 1.4 times for integrated luminosity of 2500  $fb^{-1}$ . For  $Zhh$  at  $m_h = 125.09$  GeV and  $150 \leq m_H \leq 250$  GeV signal significance is highest and almost constant. And in that region signal significance on an average increases by 51% from 1000 to 2500  $fb^{-1}$ . As  $h$  is the SM Higgs already observed that is why the observability of  $H$  in  $150 \leq m_H \leq 250$  GeV region is proposed. For  $ZHH$  signal significance is highest in the mass range  $175 \leq m_H \leq 200$  GeV at 1000  $fb^{-1}$  and in the mass range  $175 \leq m_H \leq 225$  GeV at 2500  $fb^{-1}$ . Signal significance increases by 34% in the range  $175 \leq m_H \leq 200$  GeV region and by 100% at  $m_H = 225$  GeV from 1000 to 2500  $fb^{-1}$ . For  $ZAA$  signal significance is highest at  $m_A = 175$  GeV for both 1000 and 2500  $fb^{-1}$ . And at this value signal significance increases up to 86% from 1000 to 2500  $fb^{-1}$ . It is expected that the proposed analysis will help those who are working on the observability of neutral Higgs bosons in 2HDM.

## XII. ACKNOWLEDGEMENTS

We gratefully acknowledge support from the Simons Foundation and member institutions. The current submitted version of manuscript is available on arXiv pre-prints home page <https://arxiv.org/pdf/2110.03919.pdf> arXiv:2110.03919

## XIII. STATEMENTS AND DECLARATIONS

### Funding

The authors declare that no funds, grants, or other support were received during the preparation of this manuscript.

### Competing Interests

The authors have no relevant financial or non-financial interests to disclose.

### Availability of data and materials

Data sharing not applicable to this article as no datasets were generated or analysed during the current study.

- 
- [1] P. W. Higgs, "Broken Symmetries and the Masses of Gauge Boson", Phys.Rev.Lett.13 (1964) 508-509.
  - [2] P. W. Higgs, "Broken symmetries, mass less particles and gauge fields", Phys. Lett. 12 (1964) 132-133.
  - [3] F. Englert and R. Brout, "Broken Symmetry and the Mass of Gauge Vector Mesons", Phys. Rev. Lett. 13 (1964) 321-323.
  - [4] R. S. Gupta, H. Rzehak and J. D. Wells, "How well do we need to measure the Higgs boson mass and self-coupling", Phys. Rev. D 88 (2013) 055024, arXiv:1305.6397 [hep-ph].
  - [5] G. C. Branco, P. M. Ferreira, L. Lavoura, M. N. Rebelo, M. Sher, and J. P. Silva, Phys. Rept. 516, 1 (2012), arXiv:1106.0034 [hep-ph].
  - [6] T. D. Lee, Phys. Rev. D8, 1226 (1973).
  - [7] S. L. Glashow and S. Weinberg, Phys. Rev. D15, 1958 (1977).
  - [8] G. C. Branco, Phys. Rev. D22, 2901 (1980).
  - [9] J. Mrazek, A. Pomarol, R. Rattazzi, M. Redi, J. Serra, and A. Wulzer, Nucl. Phys. B853, 1 (2011), arXiv:1105.5403 [hep-ph].

- [10] S. Davidson and H. E. Haber, Phys. Rev. D72, 035004 (2005), [Erratum: Phys. Rev.D72,099902(2005)], arXiv:hep-ph/0504050 [hep-ph].
- [11] M. Aoki, S. Kanemura, K. Tsumura, and K. Yagyu, Phys. Rev. D80, 015017 (2009), arXiv:0902.4665 [hep-ph].
- [12] M. D. Campos, D. Cogollo, M. Lindner, T. Melo, F. S. Queiroz, and W. Rodejohann, JHEP 08, 092 (2017), arXiv:1705.05388 [hep-ph].
- [13] S. Kanemura, E. Senaha, T. Shindou and T. Yamada, "Electroweak phase transition and Higgs boson couplings in the model based on supersymmetric strong dynamics", JHEP 1305 (2013) 066, arXiv:1211.5883 [hep-ph].
- [14] A. Gutierrez-Rodriguez, M. A. Hernandez-Ruiz, O. A. Sampayo, A. Chubykalo and A. Espinoza-Garrido, The Triple Higgs Boson Self-Coupling at Future Linear  $e^+e^-$  Colliders Energies: ILC and CLIC, J. Phys. Soc. Jap. 77 (2008) 094101, [0807.0663].
- [15] M. Battaglia, E. Boos and W.M. Yao, Studying the Higgs potential at the  $e^+e^-$  linear collider, eConf C010630 (2001) E3016, [hep-ph/0111276].
- [16] D. d'Enterria, Physics at the FCC-ee, in Proceedings, 17th Lomonosov Conference on Elementary Particle Physics: Moscow, Russia, August 20-26, 2015, pp. 182–191, 2017,1602.05043, DOI.
- [17] C. Castanier, P. Gay, P. Lutz and J. Orloff, Higgs self coupling measurement in  $e^+e^-$  collisions at center-of-mass energy of 500-GeV, hep-ex/0101028.
- [18] A. Arhrib, R. Benbrik and C.-W. Chiang, Probing triple Higgs couplings of the Two Higgs Doublet Model at Linear Collider, Phys. Rev. D77 (2008) 115013, [0802.0319].
- [19] G. Ferrera, J. Guasch, D. Lopez-Val and J. Sola, Triple Higgs boson production at the ILC within a generic Two-Higgs-Doublet Model, PoS RADCOR2007 (2007) 043, [0801.3907].
- [20] G. Ferrera, J. Guasch, D. Lopez-Val and J. Sola, Triple Higgs boson production in the Linear Collider, Phys. Lett. B659 (2008) 297–307, [0707.3162].
- [21] A. Djouadi, W. Kilian, M. Muhlleitner and P. M. Zerwas, Testing Higgs selfcouplings at  $e^+e^-$  linear colliders, Eur. Phys. J. C10 (1999) 27–43, [hep-ph/9903229].
- [22] M. N. Dubinin and A. V. Semenov, Triple and quartic interactions of Higgs bosons in the general two Higgs doublet model, hep-ph/9812246.
- [23] M. N. Dubinin and A. V. Semenov, Triple and quartic interactions of Higgs bosons in the two Higgs doublet model with CP violation, Eur. Phys. J. C28 (2003) 223–236, [hep-ph/0206205].
- [24] G. Chalons, A. Djouadi and J. Quevillon, The neutral Higgs self-couplings in the (h)MSSM, Phys. Lett. B780 (2018) 74–80, [1709.02332].
- [25] F. Boudjema and A. Semenov, Measurements of the SUSY Higgs selfcouplings and the reconstruction of the Higgs potential, Phys. Rev. D66 (2002) 095007, [hep-ph/0201219].
- [26] J. Gao, CEPC-SppC Towards CDR, in Proceedings, 8th International Particle Accelerator Conference (IPAC 2017): Copenhagen, Denmark, May 14-19, 2017, p. WEPIK016, 2017,

DOI.

- [27] CEPC-SPPC Study Group collaboration, Z. Liang, Electroweak Physics at CEPC, PoS ICHEP2016 (2016) 692.
- [28] M. Xiao, J. Gao, D. Wang, F. Su, Y.-W. Wang, S. Bai et al., Study of CEPC performance with different collision energies and geometric layouts, Chin. Phys. C40 (2016) 087001, [physics.acc-ph/1512.07348].
- [29] Future circular collider study, <http://cern.ch/fcc-ee/>
- [30] TLEP Design Study Working Group collaboration, M. Bicer et al, First Look at the Physics Case of TLEP, JHEP 01 (2014) 164, [hep-ex/1308.6176].
- [31] LCC collaboration, A. Yamamoto, International Linear Collider (ILC) - Technical Progress and Prospect -, PoS ICHEP2016 (2017) 067.
- [32] The Compact Linear Collider (CLIC), <https://clic.cern/>
- [33] Sanyal P. (2019). Limits on the Charged Higgs Parameters in the Two Higgs Doublet Model using CMS  $\sqrt{s}=13\text{TeV}$  Results, arXiv: 1906.02520v3 [hep-ph].
- [34] Chakraborty I. & Kundu A. (2015). On the scalar potential of two-Higgs doublet models, arXiv:1508.00702v2 [hep-ph]
- [35] S. Kanemura and K. Yagyu, Unitarity bound in the most general two Higgs doublet model, Phys. Lett. B751 (2015) 289-296, [hep-ph/1509.06060].
- [36] D. Eriksson, J. Rathsman and O. Stal (2009). 2HDMC - Two-Higgs-Doublet Model Calculator, arXiv: 0902.0851 [hep-ph].
- [37] J. F. Gunion and H. E. Haber, Cp-conserving two-higgs-doublet model: The approach to the decoupling limit, Physical Review D 67 (2003) 075019.
- [38] M. Aoki, S. Kanemura, K. Tsumura and K. Yagyu, Phys. Rev. D 80 (2009) 015017 arXiv: 0902.4665 [hep-ph].
- [39] G. Bhattacharyya and D. Das (2015). Scalar sector of Two-Higgs-Doublet models: A mini-review, arXiv:1507.06424v1 [hep-ph].
- [40] G. C. Branco, W. Grimus and L. Lavoura, "Relating the scalar flavor changing neutral couplings to the CKM matrix", Phys. Lett. B380, 119 (1996) [hep-ph/9601383].
- [41] S. L. Glashow and S. Weinberg, "Natural Conservation Laws for Neutral Currents", Phys. Rev. D15, 1958 (1977).
- [42] S. F. Novaes, Standard model: An Introduction, in Particles and fields. Proceedings, 10th Jorge Andre Swieca Summer School, Sao Paulo, Brazil, February 6-12, 1999, pp. 5–102, 1999, hep-ph/0001283.
- [43] G. C. Branco, P. M. Ferreira, L. Lavoura, M. N. Rebelo, M. Sher and J. P. Silva, Theory and phenomenology of two-Higgs-doublet models, arXiv:1106.0034 [hep-ph].
- [44] Craig, Nathaniel; Galloway, Jamison; Thomas, Scott (2016). "CP-Violation in the Type-III Natural-Flavor-Conserving 2HDM". arXiv:1612.02891v3 [hep-ph].

- [45] Two-Higgs-doublet model, <https://en.wikipedia.org/wiki/Two-Higgs-Doublet-model>
- [46] N. Sonmez (2018). Measuring the triple Higgs self-couplings in two Higgs doublet model, arXiv: 1806.08963v4.
- [47] I.F. Ginzburg and I.P. Ivanov (2018). Tree-level unitarity constraints in the 2HDM with CP-violation, arXiv: hep-ph/0312374v1.
- [48] T. Enomoto and R. Watanabe, Flavor constraints on the Two Higgs Doublet Models of  $Z_2$  symmetric and aligned types, JHEP 05 (2016) 002, [1511.05066].
- [49] S. Moretti, 2HDM Charged Higgs Boson Searches at the LHC: Status and Prospects, PoS CHARGED2016 (2016) 014, [1612.02063].
- [50] M. E. Peskin and T. Takeuchi, A New constraint on a strongly interacting Higgs sector, Phys. Rev. Lett. 65 (1990) 964–967.
- [51] M. E. Peskin and T. Takeuchi, Estimation of oblique electroweak corrections, Phys. Rev. D46 (1992) 381–409.
- [52] H. E. Haber and D. O’Neil, Basis-independent methods for the two-Higgs-doublet model III: The CP-conserving limit, custodial symmetry, and the oblique parameters S, T, U, Phys.Rev. D83 (2011) 055017, [1011.6188].
- [53] J. F. Gunion and H. E. Haber, Cp-conserving two-higgs-doublet model: The approach to the decoupling limit, Physical Review D 67 (2003) 075019.
- [54] W. Grimus, L. Lavoura, O. M. Ogreid and P. Osland, The Oblique parameters in multi-Higgs-doublet models, Nucl. Phys. B801 (2008) 81–96, [0802.4353].
- [55] N. Polonsky and S. Su, More corrections to the Higgs mass in supersymmetry, Phys. Lett.B508 (2001) 103–108, [hep-ph/0010113].
- [56] T. Enomoto and R. Watanabe, Flavor constraints on the Two Higgs Doublet Models of  $Z_2$  symmetric and aligned types, JHEP 05 (2016) 002, [hep-ph/ 1511.05066].
- [57] S. Moretti, 2HDM Charged Higgs Boson Searches at the LHC: Status and Prospects, PoS CHARGED 2016 (2016) 014, [hep-ph/1612.02063].
- [58] M. E. Peskin and T. Takeuchi, A New constraint on a strongly interacting Higgs sector, Phys. Rev. Lett. 65 (1990) 964-967.
- [59] M. E. Peskin and T. Takeuchi, Estimation of oblique electroweak corrections, Phys. Rev. D46 (1992) 381-409.
- [60] H. E. Haber and D. O’Neil, Basis-independent methods for the two-Higgs-doublet model III: The CP-conserving limit, custodial symmetry, and the oblique parameters S,T, U, Phys. Rev. D83 (2011) 055017, [hep-ph/1011.6188].
- [61] W. Grimus, L. Lavoura, O. M. Ogreid and P. Osland, The Oblique parameters in multi-Higgs- doublet models, Nucl. Phys. B801 (2008) 81-96, [hep-ph/0802.4353].
- [62] A.Belyaev, N.Christensen,A.Pukhov. ”CalcHEP 3.4 for collider physics within and beyond the Standard Model”, Computer Physics Communications 184 (2013), pp. 1729-1769, DOI

information: 10.1016/j.cpc.2013.01.014 arXiv:1207.6082.

- [63] T. Sjostrand, S. Mrenna, P.Z. Skands, Comput. Phys. Commun. 178, 852 (2008). arXiv:0710.3820
- [64] M. Dobbs and J.B. Hansen, The HepMC C++ Monte Carlo event record for High Energy Physics (Comput. Phys. Commun. 134 (2001) 41).
- [65] M. Cacciari, in Deep inelastic scattering. Proceedings, 14th International Workshop, DIS 2006, Tsukuba, Japan, April 20-24, 2006, vol. 125, pp. 487-490 (2006). arXiv:hep-ph/0607071 46. M. Cacciari, G.P. Salam, G. Soyez, Eur. Phys. J. C 72, 1896 (2012). arXiv:1111.6097.
- [66] FastJet: M. Cacciari, G.P. Salam, G. Soyez, Eur. Phys. J. C 72, 1896 (2012). arXiv:1111.6097.
- [67] R. Brun, F. Rademakers, Nucl. Instrum. Meth. A389, 81 (1997).